

## 2. ACCELERATOR AUGMENTATION PROGRAM

### 2.1 LINAC

S.Ghosh, B.K.Sahu, A.Rai, P.Patra, G.K.Chowdhury, A.Pandey, D.S.Mathuria, J.Karmakar, S.S.K.Sonti, K.K.Mistry, R.N.Dutt, A.Sarkar, R.Joshi, R. Ahuja, R. Kumar, S.K.Suman, J.Chacko, A.Chowdhury, S.Kar, S.Babu, M.Kumar, J.Antony, J.Zacharias, P.N.Prakash, T.S.Datta, and D.Kanjilal

#### 2.1.1 Status report and improvements carried out in operational Superconducting (SC) Linac

In the year 2012-13, for the first time at IUAC, all the three accelerating modules along with the superbuncher and rebuncher were operational for about three months. During this time, the ion beams from Pelletron accelerator were further accelerated by the linac and delivered for scheduled experiments. As many resonators underwent cold test for the first time, accelerating fields measured for a few of them were not up to the mark ( $< 3$  MV/m). It was felt that more surface treatment would be necessary to improve their performance.

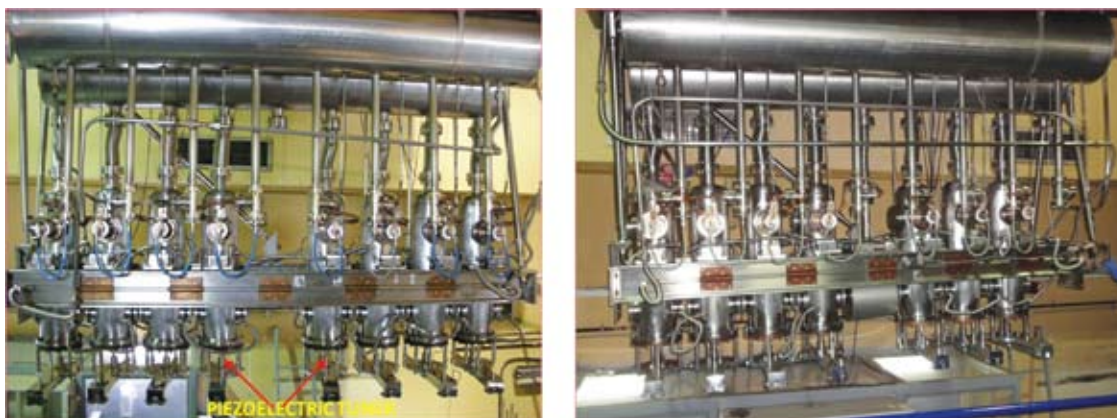


Fig. 1. The second (a) and third (b) accelerating linac modules with the gas based mechanical tuning system replaced by the piezo actuator based tuning mechanism.

So the resonators with poor performance (accelerating fields  $< 2$  MV/m) underwent more electropolishing cycles followed by hour long ultrasonic rinsing by de-ionized water at  $65^{\circ}$  C. A number of resonators with reasonably better performance ( $> 2$  MV/m) were only subjected to ultrasonic rinsing by the same ultra-pure water.

During the last linac operation, in the third linac accelerating module, mechanical frequency tuning by piezoelectric actuator was tested on a few resonators and their performance was found to be excellent. After the successful test of the piezo tuner, the gas based tuning mechanism installed in all the resonators of the second and the third accelerating modules were replaced by piezo tuner (figure 1). The electronic control module including HV power supply for the piezoelectric actuators were also developed in-house and installed in all the sixteen resonators of the second and the third modules.

Cooling arrangement for the power coupler, already installed in the resonators of the third module, was also implemented in all the eight resonators of linac-2. Drive coupler cables of the resonators of linac-2 were replaced by high power cables with higher temperature rating insulation. The new modifications to provide extra protection to the power coupler and the cable would help increase the accelerating field of the resonators. Now, the complete linac is ready for beam acceleration scheduled in the summer of 2014.

### **2.1.2 New developments associated with superconducting linac**

#### **A. Installation of a couple of class-100 clean rooms for high pressure rinsing facility and resonator assembly**

It was felt that the high pressure rinsing of the resonators should be done prior to their installation in the cryostat and the rinsing facility should be located close-by. To implement this idea, a couple of class-100 rooms with the high pressure rinsing facility with deionized water (18 M $\Omega$ -cm) and a high pressure pump (80 bars) are being installed in front of the linac cryostat. After high pressure rinsing, the resonators will be dried up in the same room and then these will be taken to the adjacent class-100 clean room for mounting the power coupler, pickup, mechanical tuner etc. Next the resonators, with all the ports covered by its accessories, will be brought to the third room (~ class 5000) to mount those in the cryostat.

#### **B. Modification of the existing pneumatic frequency tuner in all the eight resonators of first accelerating module**

The present pneumatic frequency tuner connected with all the eight resonators in the first accelerating module has a combination of proportional flow control valve along with an on/off solenoid valve for flow control. There is large hysteresis in operation of the proportional valve which is responsible for gas flow control. Due to this, the system becomes non-linear and the response time is very slow (~sec). Due to lack of space, the pneumatic tuning mechanism operated in the first module can't be replaced by the piezo actuator based tuning mechanism. So, to improve the dynamics of the existing tuner, a new gas flow control scheme using pulse operated proportional valves has been developed and tested. The new control scheme consists of two pulse operated proportional valves. The pulse width modulation (PWM) technique has been introduced in the control circuit and the feedback control is found to be linear and stable. The system has been tested successfully with a superconducting resonator in the test cryostat and an improvement in the dynamic response is observed. This scheme will be implemented in all the resonators of first accelerating module in the next linac operation.

#### **C. Auto phase locking mechanism for resonators in Linac-1**

During linac operation, the rate of frequency unlocking of a single SC resonator, out of total twenty five, has been found to be once in every 6-8 hours. The re-locking of the resonator needs human intervention and often becomes skill dependent. So, an improved mechanism of auto locking of the SC resonators has been developed and is being tested. In this mechanism, once the resonator is gone out of lock, the digital electronic system will track the frequency of the resonator and control the gas based tuning system to bring the frequency close to the Master Oscillator. Once the frequency is brought near the reference frequency, the frequency/phase feedback will be switched on automatically and the resonator will be captured in locked condition. The system is going to be implemented on all the eight resonators of linac-1 during the upcoming linac operation in the summer of 2014.

#### **D. Display panel for resonator status display in control room**

During ion beam acceleration through linac, continuous monitoring of the lock status of the resonators is required. Although monitoring is done from operator console in the control room, an additional diagrammatic display of the lock status offers gives an added advantage. So, a status display panel for all the 27 resonators distributed in five cryostats is being designed. The status of the accelerating cavity along with lock condition is displayed using suitable logic circuits and LEDs. There is a provision for audio alarm to warn the operator during unlocking of a cavity. The display panel will be operational during the upcoming linac operation.

### 2.1.3 Superconducting Niobium Resonators

P.N.Prakash, S.S.K.Sonti, K.K.Mistri, A.Rai, J.Sacharias, J. Antony, D.Kanjilal and A.Roy

The low beta resonator, designed and prototyped for the superconducting low beta module which will be a part of the proposed high current injector (HCI) program, was tested at 4.2 K. The resonator easily exceeded the nominal design goal of 5 MV/m with 6 W of input power. Fabrication of the two SSR1 - Single Spoke Resonators for Project-X of Fermi National Accelerator Laboratory (FNAL) progressed very well. A 650 MHz,  $\beta=0.9$  single cell niobium cavity has been successfully developed as a collaborative project between RRCAT, Indore and IUAC. In cold tests at 2 K this cavity exceeded the design goal of 17 MV/m accelerating gradient with  $Q_0 > 3 \times 10^{10}$ . Initial technical discussions for developing a 650 MHz,  $\beta=0.6$  single cell niobium cavity as a collaborative project between Variable Energy Cyclotron Centre (VECC), Kolkata and IUAC, has started.

#### 2.1.3.1 Low Beta Resonator

The superconducting niobium low beta resonator, designed and prototyped for the low beta module, that will be a part of the High Current Injector (HCI) project, was tested at 4.2 K to check its performance. The resonator is shown in figure 2.

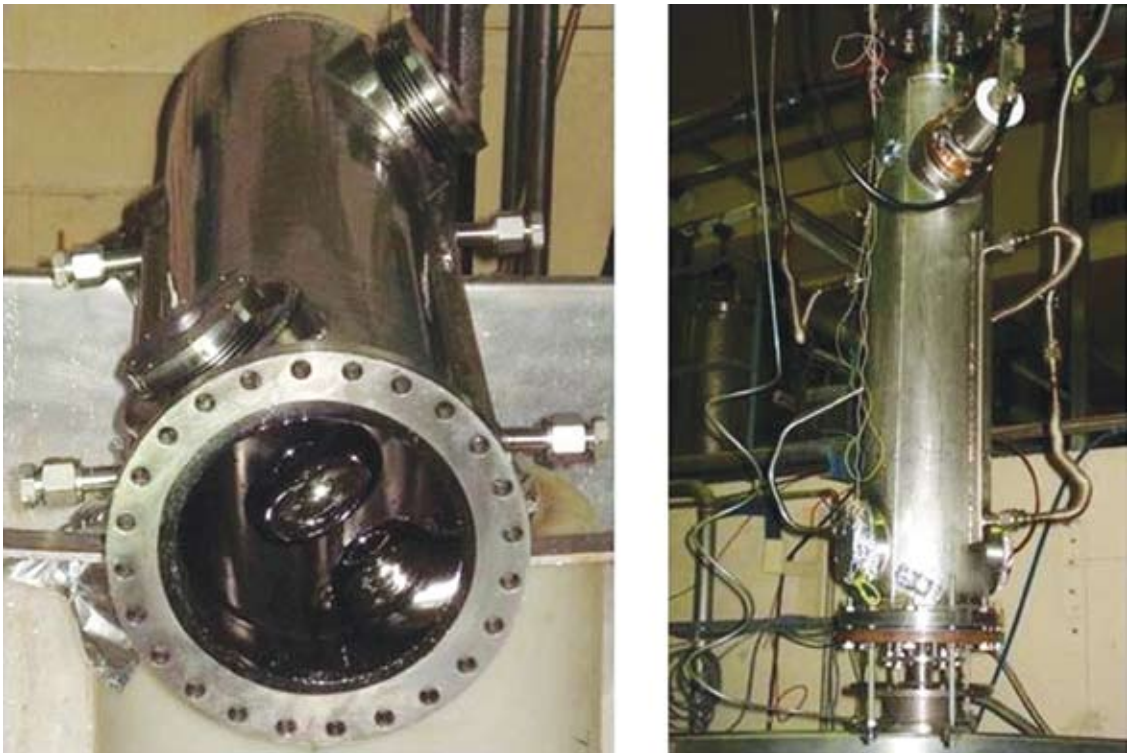


Fig. 2: Prototype niobium low beta resonator during the final stages of its surface preparation (left) and ready to be lowered in the test cryostat for cold tests (right).

In the first test at 4.2 K, the resonator easily achieved 5 MV/m accelerating gradient with 6 W of RF input power with just 30 minutes of high power pulse conditioning at 25% duty cycle, reaching a maximum gradient of 8.1 MV/m. The resonator could be conditioned through the low level multipacting barriers in less than two hours. So multipacting was not a major issue, as is expected in this design. The tuning range of the slow tuner was measured to be  $\sim 65$  kHz for a pressure change of 20 psi in the niobium slow tuner bellows. This range is slightly lower than the expected value ( $\sim 80$  kHz). This may be due to the use of a thicker gasket for mounting slow tuner bellows, resulting in the slow tuner to drift tube gap to increase.

Initial attempts to lock the resonator using the control module (that is used for controlling the Quarter Wave Resonators [QWR] in the linac) indicated that locking should be quite easy in the present design.

Even though the performance of the resonator met the nominal design goal, we strongly believe that the present design of the low beta resonator can achieve much higher gradients. So we propose to test the resonator again after another round of surface treatment to remove 40-50  $\mu\text{m}$  from the surface.

### 2.1.3.2 Single Spoke Resonators

Fabrication of the two Single Spoke Resonators – SSR1 ( $\beta=0.22$ ,  $f=325$  MHz) for Project-X of Fermi National Accelerator Laboratory (FNAL), USA, progressed very well. This year the spoke assembly was completed, electropolished and subsequently attached to the outer niobium shell. In figure 3, the spoke assembly is shown. The electropolished spoke was attached to the shell that had already been completed and electropolished earlier. The assembly of the spoke to shell collar was a challenging task. In figure 4, the shell and spoke assembly is shown.

The SSR1s will next be tuned to the correct warm frequency and the two end walls (already completed) will be attached to the outer shell. Finally the stiffening ribs will be attached on the outer shell. We are planning to complete the works in the next 6-8 weeks and ship the resonators to Fermi Lab.



Fig. 3: Spoke assembly after completion but before electropolishing (left) and electropolished spoke assembly (right) ready for attachment to the Shell.



Fig. 4: Spoke assembly after electron beam welding to the outer niobium shell.

### 2.1.3.650 MHz, $\beta=0.9$ Cavity

The accelerator design for Project-X at FNAL has been changed, and it now incorporates 650 MHz cavities in place of the 1.3 GHz TESLA-type cavities. In view of this, RRCAT and IUAC decided to jointly develop a 650 MHz,  $\beta=0.9$  single cell niobium cavity as a first step. In figure 5, the 650 MHz single cell niobium cavity is shown.



Fig. 5: First 650 MHz,  $\beta=0.9$  single cell niobium cavity built in India.

In cold tests conducted at Fermi Lab, the 650 MHz single cell cavity exceeded the design goal and achieved 19.3 MV/m accelerating gradient at a quality factor ( $Q_0$ )  $>3 \times 10^{10}$ . In figure 6, the Q-curve is shown.

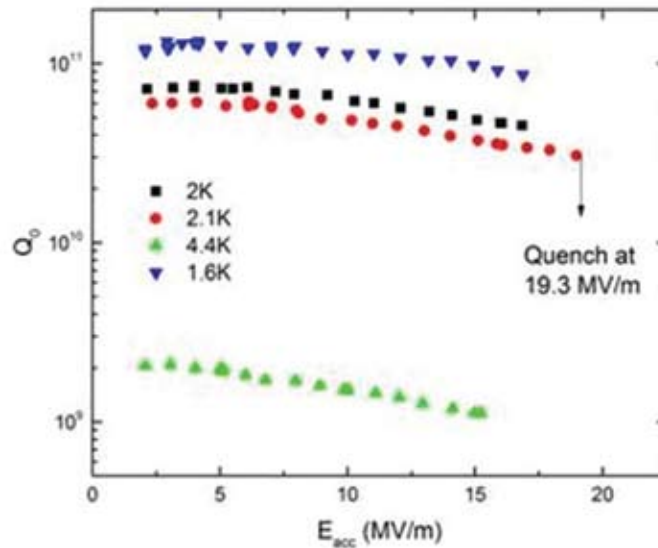


Fig. 6: Quality factor ( $Q_0$ ) as a function of accelerating gradient ( $E_{acc}$ ) at different temperatures, for the 650 MHz,  $\beta=0.9$  single cell niobium cavity.

#### **2.1.3.4 Upgradation**

The facilities for constructing superconducting niobium resonators at IUAC were commissioned more than twelve years ago. In order to maintain the capability for continuous improvement for the development of new resonator designs, and also to face newer challenges, the major facilities are being upgraded. In this regard, the electron beam welding facility is being upgraded to operate on a more modern PC with touch screen and control software supported by a new CNC system and associated PLCs. In addition, it is planned to completely overhaul the electron gun, vacuum system, various mechanical systems and other associated electronics. A new colour camera with recording facility will replace the existing system. A control box with pendant to jog the various movements will also be attached. The upgradation work will commence in September and will take approximately 4-6 weeks to complete.

In addition, we propose to upgrade the high vacuum furnace by completely overhauling the system, interlocks, vacuum pumps, cooling circuit, and by replacing the existing control system with a more modern software and hardware. It is also proposed to attach a dedicated RGA on the system for online monitoring of the gases during the heating cycle.

Similarly, it is proposed to reorganize the surface preparation laboratory (by making some changes through civil works) to reduce the dust levels inside the lab and to provide additional space for a sink and a new dedicated high pressure rinsing system. For this, a new high capacity ultrapure DI water system has been commissioned, and a modern control system based on a new PC with touch screen and PLCs has also been incorporated. The other major works will be taken up after the civil works are over.

## **2.2 HIGH TEMPERATURE SUPERCONDUCTING ECRIS -PKDELIS AND LOW ENERGY BEAM TRANSPORT (LEBT)**

G. Rodrigues, Y. Mathur, Narender Kumar, P. Barua, A. Kothari, R.Becker<sup>1</sup>, R.W. Hamm<sup>2</sup>, R.Baskaran<sup>3</sup>, R.Ahuja, Sarvesh Kumar, U.K. Rao, P.S.Lakshmy, Kedar Mal, R.N.Dutt, A.Mandal, D.Kanjilal and A. Roy

<sup>1</sup>Institut fur Angewandte Physik der Universitaet, D-60054 Frankfurt/M, Germany

<sup>2</sup>R&M Technical Enterprises, Inc., 4725 Arlene Place, Pleasanton, California 94566, USA

<sup>3</sup>Indira Gandhi Centre for Atomic Research, Kalpakkam, Tamilnadu, India

### **2.2.1**

#### **A. 18 GHz High Temperature Superconducting ECR ion source, PKDELIS and LEBT**

The source and its entire low energy beam transport have been disassembled and most of the components have been shifted to beam hall III for installation on the 100 kV high voltage platform. The basic layout of the source and the low energy beam transport on the 100 kV high voltage platform is discussed in detail in section D.

#### **B. Electronics and related maintenance activities:**

The HTS electronics in HTS-ECR, PKDELIS which is a major task force and 'heart' of the system to keep the HTS coils protected, keep a continuous check on various parameters of solenoid coils like coil temperature, voltage at various points of coils, current through coils, etc. It monitors these parameters continuously and force the coils' power supply to trip if any of the parameters crosses the threshold. We faced one problem where although all the coil parameters were ok, the HTS electronics were tripping the power supply depicting some time, the voltage tap errors at some point, or sometimes coil over temperature. It was observed that the module at slot no. 12 was not functioning properly. We diagnosed that the isolation amplifier IC ISO120P was not functioning properly and this was triggering false tripping. The IC was replaced which solved the problem.



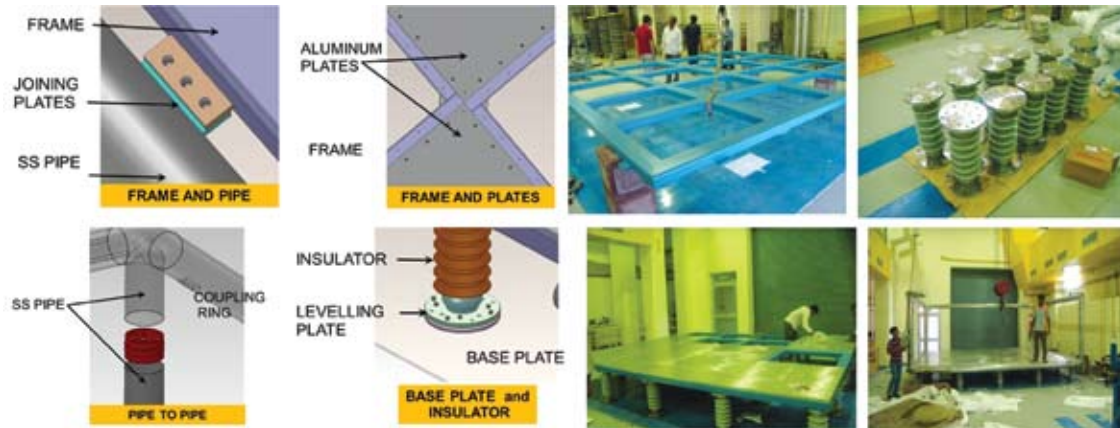


Fig. 8 : (left) Different joints ; (right) stages during installation



Fig. 9. View of 100 kV high voltage platform installed in beam hall III

## F. 2.45 GHz microwave ion sources

### a) Studies on the effect of the axial magnetic field on X-ray bremsstrahlung in a 2.45 GHz permanent magnet microwave ion source

Due to the necessity of installation of a SNICS ion source based low energy ion beam facility in the same area where the 2.45 GHz microwave ion source and LEBT were operational, the microwave ion source and LEBT were planned to be shifted to room no. 127. Before shifting of the ion source, few experiments were carried out to study the effect of the axial magnetic field on the X-ray bremsstrahlung emission from the microwave plasma [1]. The main purpose was to study the electron energy distribution function (EEDF), because the EEDF is known very little or practically unknown in these kinds of ion sources.

Due to the relatively long beam transport line, the X-ray measurements could not be carried out through the  $0^\circ$  view port of the analyzing dipole magnet. The beam-line, after the “accel-decel”

system, was dismantled in order to position the X-ray detector close to the microwave ion source. A XR-100, CdTe X-ray detector was mounted outside the vacuum chamber and along the beam axis at the extraction side of the ion source just behind the “accel-decel” system. A thin mylar window was used on the downstream flange of the “accel-decel” system to minimize the attenuation of X-rays. The detector itself consisted of a thin (100  $\mu\text{m}$ ) beryllium window and was cooled by a thermoelectric cooler. Its maximum detection efficiency (100%) was in the range of 10 to 60 keV. Each of the X-ray spectra were acquired for a total time of 90 min due to the large distance ( $\sim 600$  mm) between the plasma electrode and the X-ray detector, keeping the “accel-decel” system in the OFF condition.

(i) **Variation with distance between the magnets**

X-ray bremsstrahlung spectra have been measured at two values of separation between the magnets at an RF power of 252 W and gas pressure of  $1.3 \times 10^{-5}$  mbar, when the distance between the microwave window and injection magnet was at the minimum (3.9 cm). Here, the injection of the microwaves occurs at the microwave window in the “under resonance” regime. In one case, the magnet rings were separated by 9 cm and in the other case they were moved closer (distance between the magnets was 4.6 cm by moving the extraction ring closer to the injection ring) and these spectra are shown in figure 10 below.

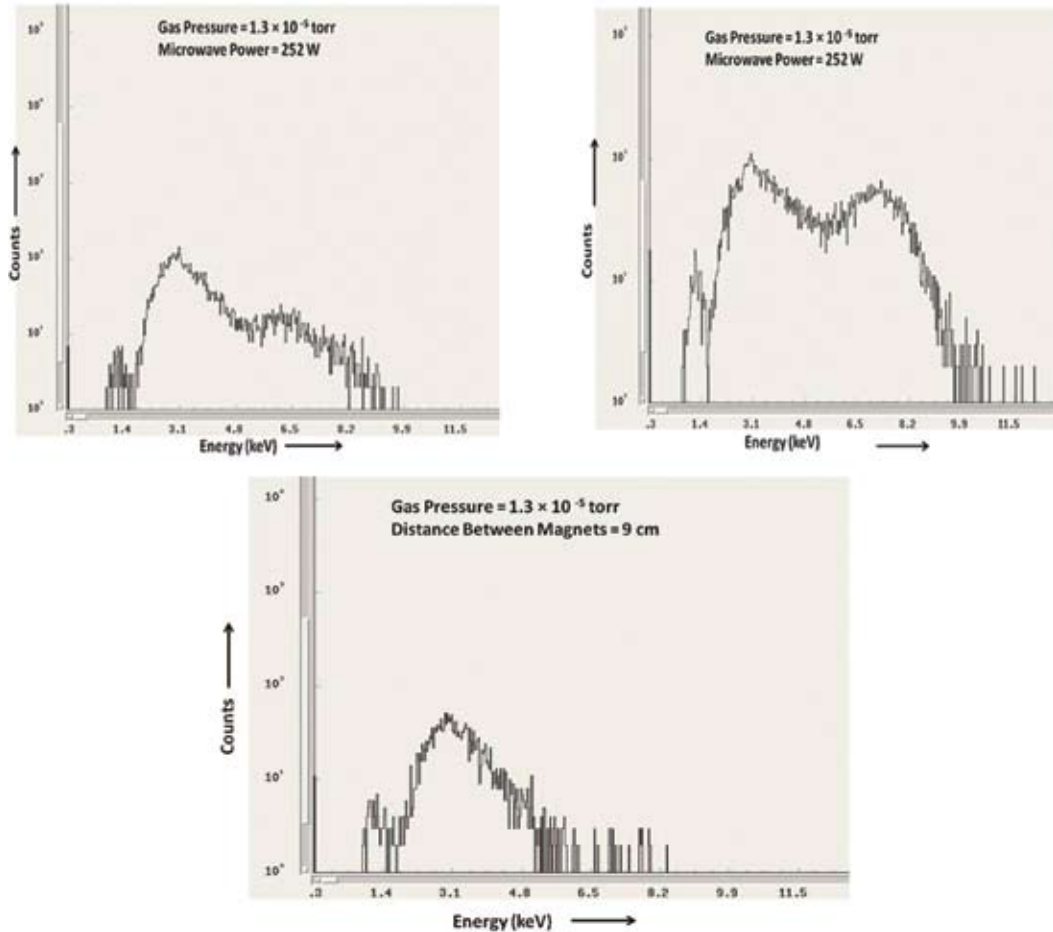


Fig. 10. X-ray spectra measured for two distances between the magnet rings (left: distance 9 cm; right: distance 4.6 cm) at 252 W ; (below) X-ray spectrum measured at 80 W, when the distance between the magnets was 9 cm.

**(ii) Variation with microwave power**

The axial magnetic field was tuned at a position keeping the two permanent rings at a distance of 9 cm, where the minimum distance between the microwave window and the injection magnet ring was kept at 3.9 cm. At three RF power levels, viz., 80, 180, and 252 W, and gas pressure of  $1.3 \times 10^{-5}$  mbar, the spectra were measured. The spectra measured at 80 and 252 W are shown on the right hand side and left hand side of figure 10, respectively. Based on the calculated ECR surface, the experimental measurements were compared with the simulations performed using TRAPCAD where  $10^5$  particles were simulated inside the whole of the plasma chamber at two RF power levels, viz., 80 W and 252 W. Calculation time was 200 ns, small enough to neglect electron-electron interactions and other collisions. The parallel and perpendicular energy components were both randomly chosen in the range 10 to 100 eV. The non-lost and lost electrons are shown on the left and right sides in figure 11. Simulation and the experimental results come to a better agreement if RF power is further increased to  $\sim 500$  W keeping the same simulation time with the default assumption of 50% of non-lost electrons.

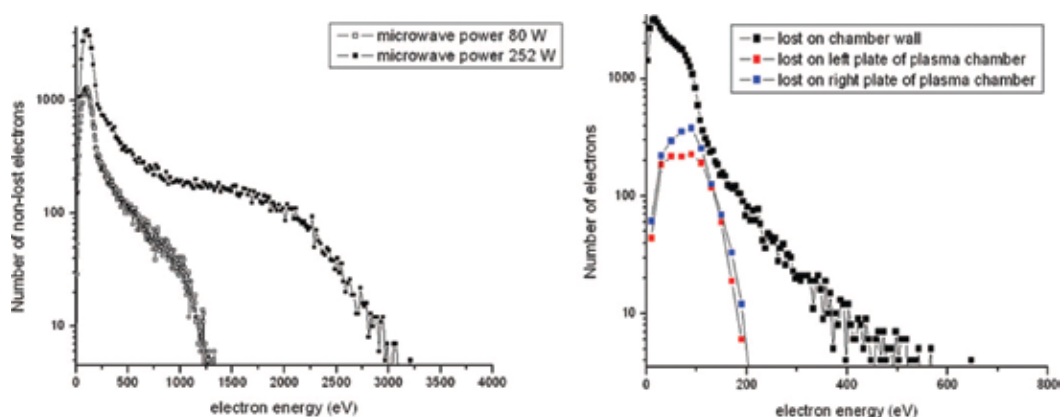


Fig. 11. (left) Simulated non-lost electrons at two RF power levels, viz., 80 and 252 W ; (right) Lost electrons at RF power 252 W.

**(iii) Variation with distance of injection magnet ring from the microwave window**

The X-ray spectra were measured by varying the distance of the injection magnet from the microwave window by keeping the distance between the magnets at 9 cm. At three distances, viz., 3.9 cm, 5 cm, and 6 cm, it was observed that the X-ray emission reduced as the distance was increased.

The X-ray bremsstrahlung measurements, obtained from the 2.45 GHz microwave ion source, showed the expected behavior when the distance between the magnets was varied and when the distance between the microwave window and the injection magnet was varied, although the intensity of the X-rays was reduced due to the large distance between the plasma electrode and the detector. The simulations of the ECR surface also showed that the ECR surface was very close to the inner radius of the plasma chamber, which was also observed experimentally. The measured energy distribution of the X-rays showed that the mean energy of the electrons was high in the case of an “under-resonance” discharge plasma. But the simulations using TRAPCAD showed that the mean energy of the electrons was much lower  $\sim 100$  eV and the lifetime of these low energy electrons was increased considerably.

**b) Design and installation of a new 2.45 GHz microwave ion source for materials science and plasma physics related experiments**

Based on the performance of the older version of a 2.45 GHz microwave ion source, a relatively

new and improved version of a 2.45 GHz , compact microwave ion source has been designed and developed with a water cooled plasma chamber and is shown in figure 12. It has been designed for providing intense beams of singly charged ions for materials science related experiments, keeping in mind the main objective of reducing the total ion implantation time required for the experiment when compared to using multiply charged ions. The plasma chamber of the ion source, due to its complexity, has been fabricated using the so-called ‘Laser Cuiusing’ technique where fine metallic powder is locally fused by a laser, and the component is built up layer by layer ( $\sim 20$  to  $60 \mu\text{m}$ ) by lowering the bottom of the installation space, applying more powder and fusing it again. It has a double walled, stainless steel plasma chamber design having an inner diameter of 90 mm and length of 101.3 mm. The cooling water can flow all over the chamber through equally-spaced ribs in between the walls. Cold and hot water are separated by a closed rib. The dimensions of the resonant cavity have been chosen to excite the  $\text{TE}_{111}$  dominant mode at 2.45 GHz. The actual length of the plasma chamber has been kept 135 mm in order to accommodate the magnet structure. Additional ports have been provided on the chamber wall for Langmuir probe plasma diagnostics.

After removing the old, air cooled microwave ion source and LEBT from room no 117, the new, water cooled, microwave ion source is presently being installed in room no. 127 on a movable rail so that maintenance and running of the source can be done easily. A wireless control system will be used for operating this facility. The additional feature of adding the gas pressure control at high voltage facilitates ease of operation and tuning of the source. The coupling of the RF power to the plasma will be done using a water cooled ridge waveguide. A short, multi electrode extraction system has been designed, fabricated and integrated with the system. to minimize the blow up of intense proton beam of 10 mA. The model calculation assumes that the ion temperatures are at  $T_i = 0 \text{ eV}$  while electron temperatures are at  $T_e = 5 \text{ eV}$ . Maximum electric fields are of the order of 60 kV/cm, which may require further optimization to minimize sparking. A compact experimental chamber with a variable size collimator and a new water cooled experimental ladder have also been designed, fabricated and installed in this facility. The ion source can be further operated at very low voltages ( $\sim 500 \text{ V}$ ) to form nano-structures. At these low operating voltages, high intensities can be extracted by utilising the secondary electrons produced for space charge compensation.

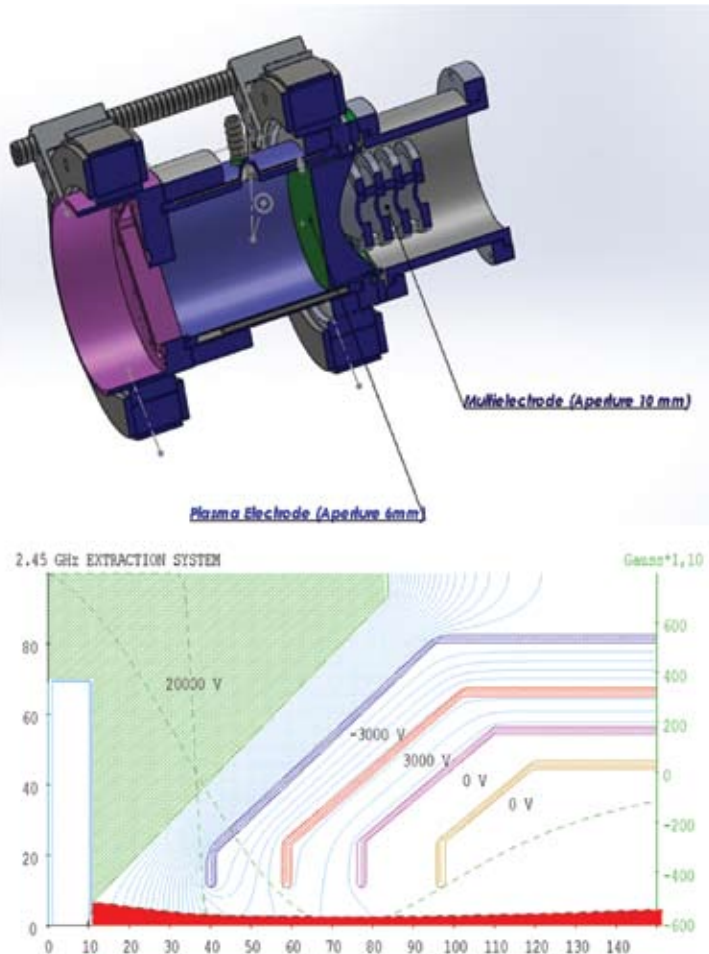


Fig. 12. (above) View of the new microwave ion source coupled to the extraction system and (below) extraction system designed for transporting 10 mA of protons

## G. Frequency tuning effect

The frequency tuning effect in ECR ion sources has become a useful technique to improve the performance of existing ion sources and was pioneered by the ECR group at Catania, Italy. Generally, the electromagnetic field distribution inside a cavity depends on the frequency and is preserved even in the presence of the plasma. Additionally, the ECR surface can get modified in terms of its dimension and shape which can further influence the beam intensity, shape, emittance and brightness. Due to remarkable changes in the beam characteristics, quality of the beam can be improved further. In the field of ECR ion source development, there is a constant endeavour to improve beam quality and intensity. Most of the earlier works done using frequency tuning has shown the influence on the beam characteristics, namely, a clear variation in the beam quality and intensity as a function of frequency. In some experiments, the formation of hollow beams was observed just after source extraction before the solenoid focusing element. It is also known that the improvement of the beam characteristics is a manifestation of the improved conditions of the plasma and the beam extraction system. Therefore, an understanding of the bremsstrahlung spectrum of cold, warm, and hot electrons and the electron distribution function is also necessary to study how characteristics of the beam are influenced by the frequency tuning. In order to further understand the frequency tuning effect on the beam characteristics and on the plasma conditions inside the cavity, it was felt necessary to study this effect on a lower frequency type of ECR ion source (here, the 10 GHz NANOGAN) where the separation between various modes in the cavity is much larger than that of a source operating at a higher frequency [2]. A set-up to measure the X-ray bremsstrahlung from the injection side of the source is shown in the bottom panel of figure 13. A model of the ECR cavity with one of the computed dominant modes,  $TE_{117}$  is shown in the top panel of figure 13. The left side of figure 14 shows the effect of the various charge states of oxygen, electron energy distributions, and reflection co-efficient as a function of frequency and the right side of figure 14 shows the effect of the various charge states of argon, electron energy distributions, and reflection co-efficient as a function of frequency. In figure 15, the measured shape of the beam for oxygen plasma for various frequencies is shown at the top and after analysis at the bottom for  $O^{5+}$  with their intensities.

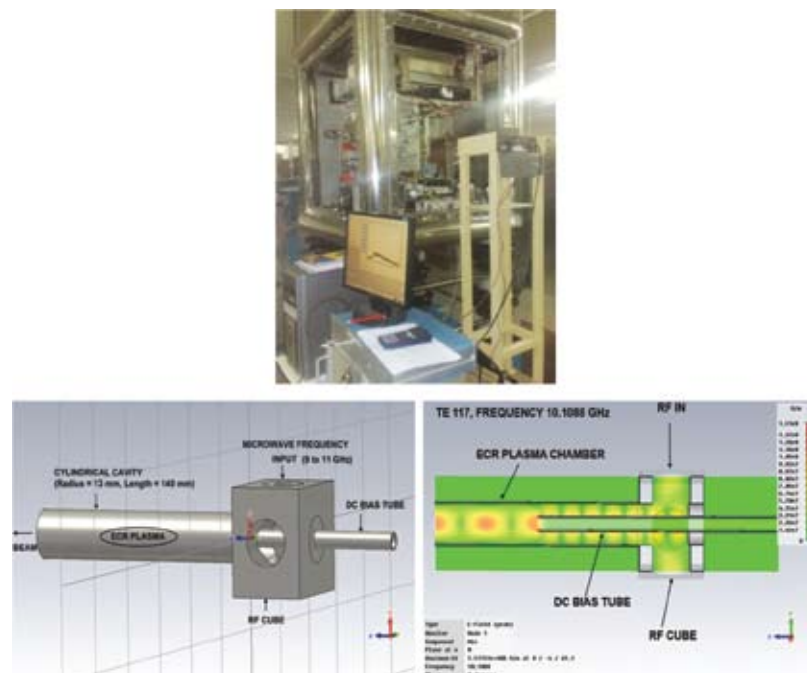


Fig. 13. (above) Set-up to measure the X-ray bremsstrahlung from the 10 GHz NANOGAN ECR ion source as a function of frequency; (left) Model of the ECR cavity with bias tube coupled to the RF cube used for the electromagnetic field calculation using CST microwave studio; (right)  $TE_{117}$  mode calculation using CST microwave studio for the ECR cavity with bias tube coupled to the RF cube.

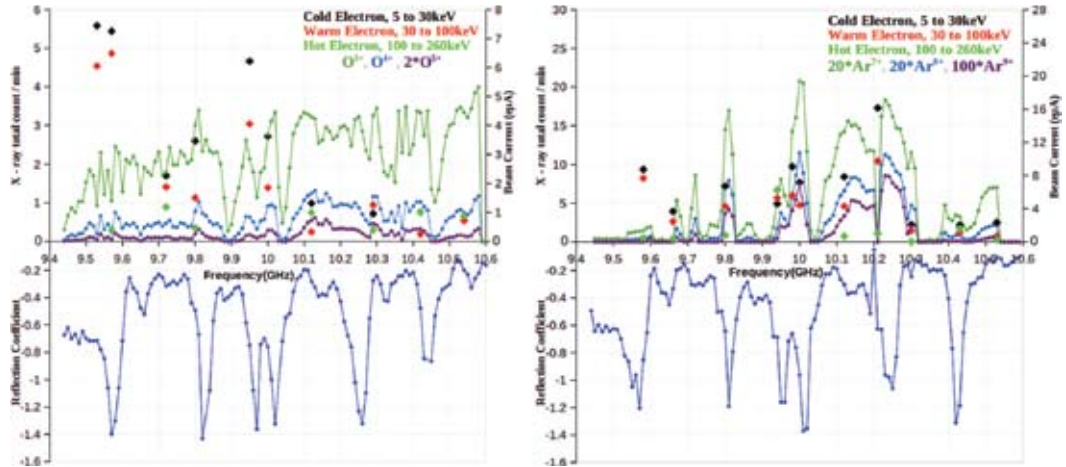


Fig. 14. (left) Effect of the various charge states of oxygen, electron energy distributions, and reflection co-efficient as a function of frequency; (right) Effect of the various charge states of argon, electron energy distributions, and reflection co-efficient as a function of frequency.

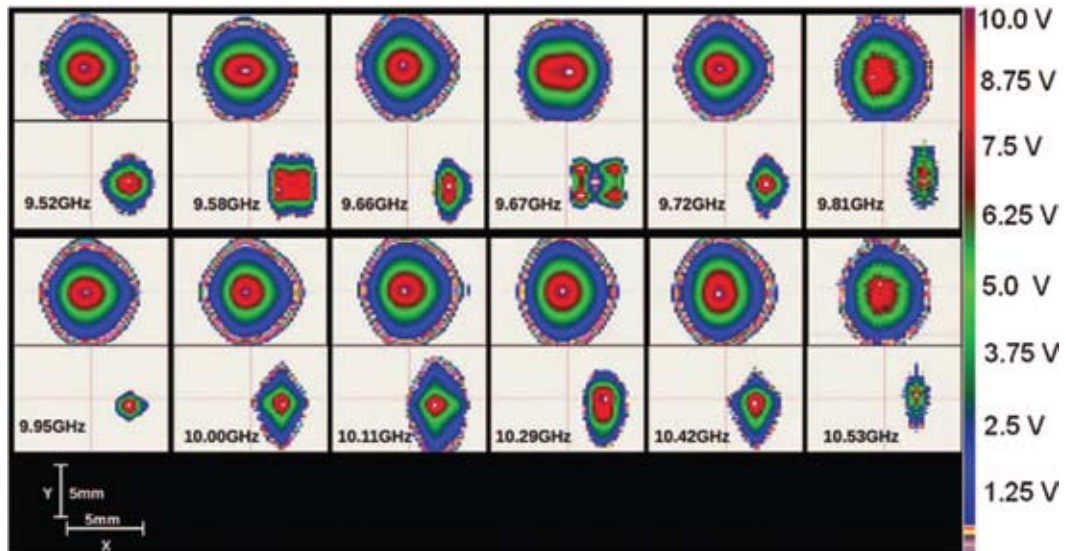


Fig. 15. (Top) Measured shape of the beam for oxygen plasma for various frequencies and (bottom) after analysis for  $O^{5+}$  with their intensities.

Considering the measurements for oxygen and argon beams, in terms of beam intensities and beam shape measurements for oxygen plasma, it is observed that there is a strong absorption of microwave power at various frequencies whenever the reflection co-efficient showed a minimum value. The effect was found to be stronger for the higher charge states. The shape of the beam as a function of frequency clearly shows a strong variation at BPM 1. The warm and cold components of the electrons were found to be directly correlated with beam intensity enhancement in case of  $Ar^{9+}$  but not so for  $O^{5+}$ . The warm electron component was, however, much smaller compared to the cold component.

#### H. Extraction of intense ion beams from a high field ECR into a RFQ channel

The ion current achievable from high intensity ECR sources for highly charged ions is limited by the high space charge. This makes classical extraction systems for the transport and subsequent matching to a radio frequency quadrupole (RFQ) accelerator less efficient. The direct plasma

injection (DPI) method, developed originally for the laser ion source, avoids these problems. It uses the combined focusing of the gap between the ion source and the RFQ vanes (or rods) and the focusing of the RF fields from the RFQ penetrating into this gap. For high performance ECR sources that use superconducting solenoids, the stray magnetic field of the source in addition to the DPI scheme, provides focusing against the space charge blow-up of the beam. A combined extraction/matching system has been designed [3] for a high performance ECR ion source injecting into an RFQ, allowing a total beam current of 10 mA from the ion source for the production of highly charged  $^{238}\text{U}^{40+}$  (1.33 mA) to be injected at an ion source voltage of 60 kV. In this design, the features of IGUN have been used to take into account the RF-focusing of an RFQ channel (without modulation), the electrostatic field between ion source extraction and the RFQ vanes, the magnetic stray field of the ECR superconducting solenoid and the defocusing space charge of an ion beam. The stray magnetic field is shown to be critical in the case of a matched beam. For a matched beam at the entrance of the RFQ-channel, the variation of the axial magnetic field gives the smallest radius for different  $q/m$  at different magnetic fields. The radius and the divergence decrease with increasing magnetic fields. Therefore, there is an optimal magnetic field for each charge state of U. In the final design shown in the top panel of figure.16, for the matching of a 1.33 mA  $^{238}\text{U}^{40+}$  beam, an optimized shape of the vane tip radius in the radial matching section was found to be necessary. A total beam intensity of 10 mA consisting of 1.33 mA of  $^{238}\text{U}^{40+}$  ions, other charge states of  $\text{U}^+$  ions and ions of the mixing gas was used to achieve a 66.66% fill of the aperture and a 50% fill of acceptance. On the bottom panel of figure.16, the current densities and rms emittances (units for 1 micron = 1 mm.mrad) of 1.33 mA of  $^{238}\text{U}^{40+}$  and mixing gas components inside the RFQ channel are shown. It is evident that the RFQ-channel may be very effective and less sensitive than a conventional extraction system for high performing ECR ion sources.

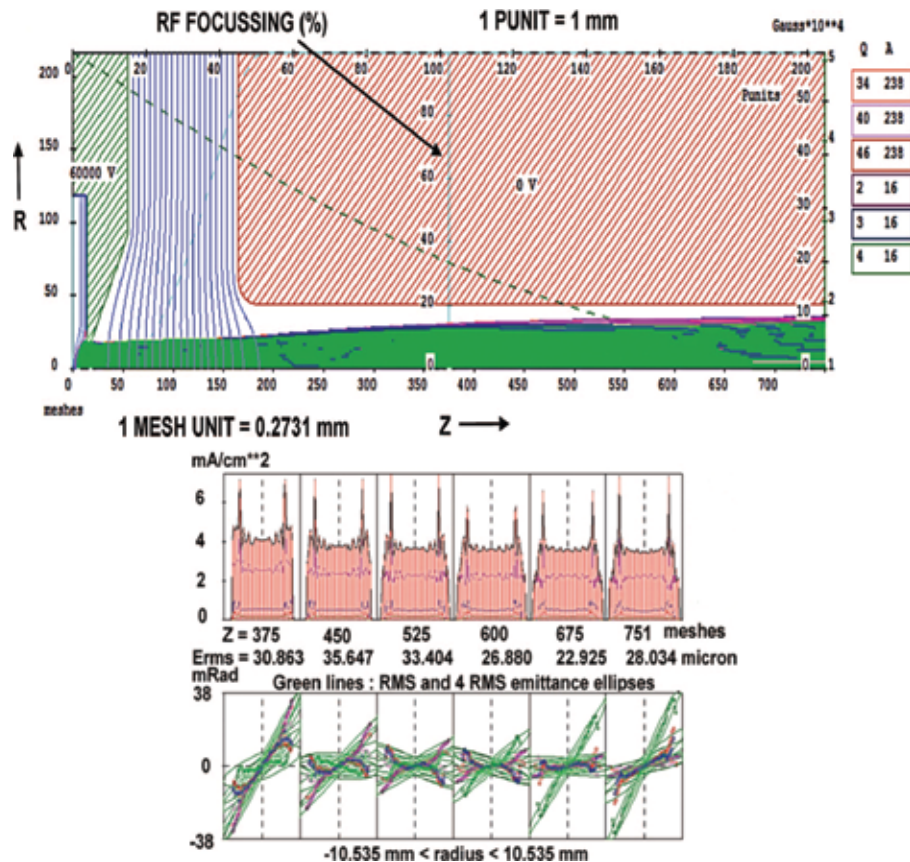


Fig. 16. (Top) Optimized design for transporting a total current of 10 mA (from 56 GHz ECR source), consisting of 1.33 mA of  $^{238}\text{U}^{40+}$ , other  $\text{U}^+$  charge states and oxygen mixing gas ions directly into an RFQ. (Bottom) Current densities and rms emittances of 1.33 mA of  $^{238}\text{U}^{40+}$ , other  $\text{U}^+$  charge states, and oxygen mixing gas components inside the RFQ channel.

It has been shown that a high performance ECR ion source can be coupled to an RFQ channel to transport intense beams of highly charged heavy ions without the problems of space charge beam blow-up and/or sparking in the extraction region. It was found that the stray magnetic field of the ECR source is critical for a matched beam. The RF focusing in IGUN shows its versatility and simplicity to directly match the beam from the ECR source to the radial matching section of the RFQ. This technique has promising applications for injecting and transporting very intense beams into RFQ accelerators for research and more efficient, compact neutron generators. The Accelerator Driven Sub-critical System (ADSS) being developed at various laboratories around the world to create nuclear energy may also benefit from this technique, both in terms of transporting intense beams of protons and making the low energy segment more compact.

## References

- [1] Studies on the effect of the axial magnetic field on the X-ray bremsstrahlung in a 2.45 GHz permanent magnet microwave ion source, *Rev.Sci.Instrum.*,85, 02C103 (2014).
- [2] Effect of frequency tuning on bremsstrahlung spectra, beam intensity, and shape in the 10 GHz NANOGAN electron cyclotron resonance ion source, *Rev.Sci.Instrum.*,85, 02A944 (2014).
- [3] The direct injection of intense ion beams from a high field electron cyclotron resonance ion source into a radio frequency quadrupole, *Rev.Sci.Instrum.*,85, 02A740 (2014).
- [4] A compact 2.45 GHz ECR ion source based high fluence facility at IUAC, Indian Particle Accelerator Conference, (INPAC) VECC, Kolkata, Nov. 19-22, ID 89 (2013).
- [5] Effect of source tuning parameters on the plasma potential of heavy ions and its influence on the longitudinal optics of the high current injector, Proceedings of the 20<sup>th</sup> International Workshop on ECR Ion Sources, September 2012, Sydney, Australia, <http://accelconf.web.cern.ch/AccelConf/ECRIS2012/>.

### 2.2.2 Radio frequency quadrupole accelerator

Rajeev Ahuja, Ashok Kothari, Sugam Kumar and C. P. Safvan

A prototype RFQ was built and low power tests including bead pull and frequency shift tests were successfully carried out earlier. Based on the results, the design of the final prototype was completed last year and fabrication of the components started. This year, we have completed fabrication of the vanes, support stems, and the base plates. The initial assembly of the components was done in the newly available Beam Hall III. Figure 17 shows the vanes and the stems as received from the Indo German Tool Room in Ahmedabad. The vanes and stems were installed for checking into the copper plated cavity (copper plating done at RRCAT, Indore). Figure 18 shows the partly assembled RFQ accelerator.



Fig. 17. Stem supports and vanes for the RFQ accelerator.

High power tests on the prototype RFQ were also done to test the design of the cooling systems. It was found that the vanes and supports were adequately cooled but the chamber itself required additional cooling arrangements due to some hot spots in the cavity. This also tested the 48.5 MHz, 30 kW RF amplifier acquired for the RFQ.

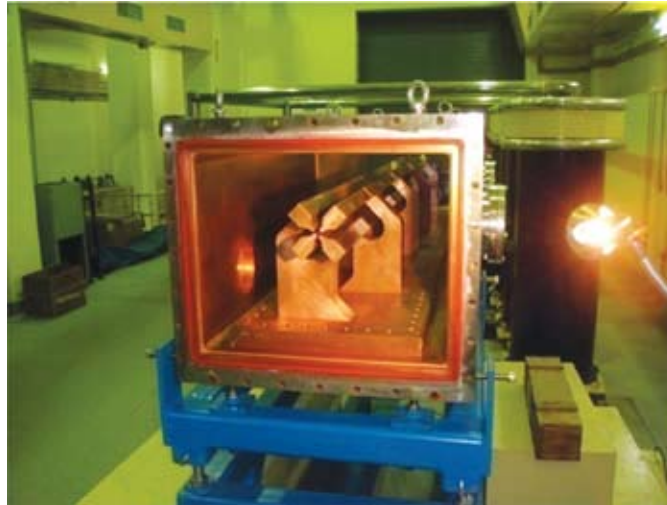


Fig. 18. Partially assembled RFQ accelerator in Beam Hall III

### 2.2.3 Drift tube linac resonator

Ajith Kumar B P, J. Sacharias, R Mehta, V V V Satyanarayana, R V Hariwal, S Kedia, Rajesh Kumar, S Venkataramanan, B K Sahu and P Barua

The High Current Injector (HCI) project at IUAC consists of an ECR source, Radio Frequency Quadrupole (RFQ) and a Drift Tube Linac (DTL) to achieve an output energy of 1.8 MeV/u, for ions having  $A/q \leq 6$ . The RFQ output energy is 180 keV/u and the DTL accelerates it further to 1.8 MeV/u. Acceleration from 180 keV/u to 1.8 MeV/u is done by six independently phased IH type RF cavities. Beam dynamics studies and the electrical design of all the resonators have been completed. The first resonator has been fabricated and tested for the accelerating field distribution and continuous operation at the designed power level.

The first resonator, an eleven gap structure, was designed to give a quality factor of 11500 and consume 5 kW of RF power to provide an effective accelerating voltage of 1 MV. Resonator pressure was around  $2.0 \times 10^{-7}$  mbar. and measured Q was around 10500. The electric field distribution, measured by a bead pull test, agreed with the design values. The resonator was powered up to 6 kW, under critically coupled condition, and operated continuously at 5 kW for 48 hours. The temperature of the tank body was kept around 25°C, during the operation. A self excited loop was used for powering the resonator to take care of the resonant frequency drifts due to change in temperature. The cavity is undergoing further tests to verify and validate various design and RF parameters. Amplitude and phase control systems will be implemented after that.

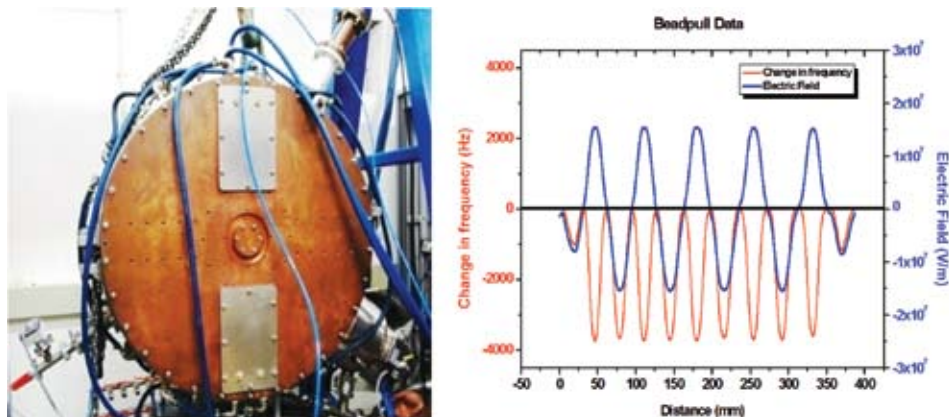


Fig. 19

## 2.2.4 Beam transport system for HCI

Sarvesh Kumar and A Mandal

This year, major thrust has been given for hardware design of beam transport system of HCI and development of the controller for multi harmonic buncher. Air cooled quadrupole magnets, steerer magnets, spiral bunchers and fast Faraday cups have been designed. Some of them have been tested. Power supplies for different magnets have been indigenously developed. Details of development activities are summarized below.

### 2.2.4.1 Beam optics of high current injector

Sarvesh Kumar and A Mandal

The overall planning of beam transport system (BTS) for HCI is given below. Figure 20 shows the number of required beam optical components in each transport section and injection energies at different location of HCI. HEBT section is the biggest section and requires maximum number of beam optical components to transport the beam as compared to LEBT and MEBT sections.

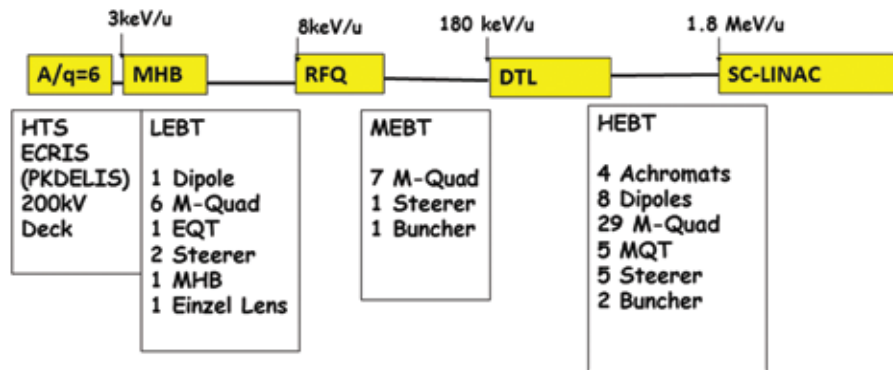


Fig. 20 Schematics of HCI beam transport system

#### I. Low energy beam transport section (LEBT)

The layout of LEBT section was fixed as per beam optics calculations by suitably inserting beam diagnostic devices, steerer magnets and vacuum pumps. Finer adjustments were made to accommodate all types of beam optical components and the beam optics was again computed using TRACEWIN code to match exactly the twiss parameters of the RFQ with LEBT section, as shown in figure 21. The corresponding placement of physical components is shown in figure 22.

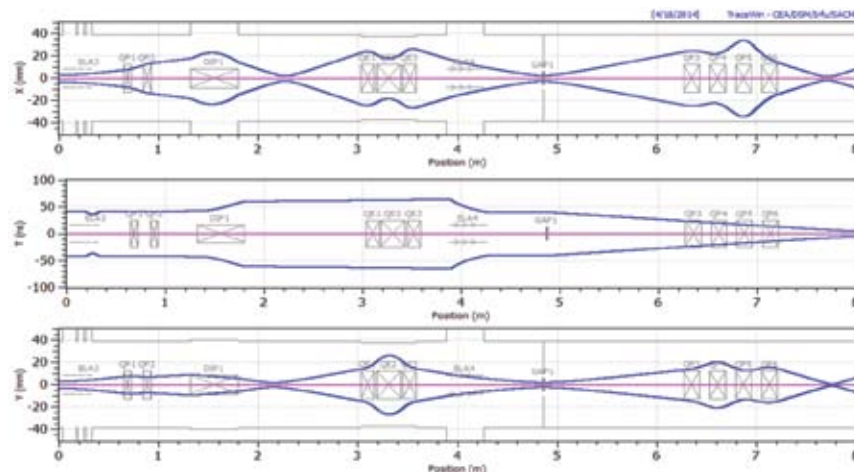


Fig. 21 Beam optics of LEBT section using TRACEWIN code

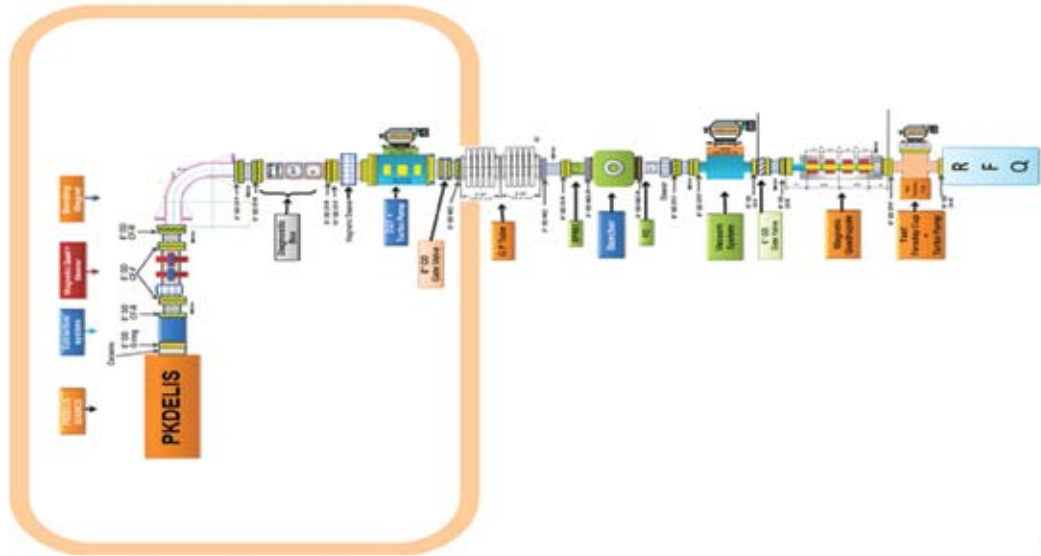


Fig. 22 Layout of the LEBT section

## II. Medium energy beam transport section (MEBT)

The ion beam accelerated by the RFQ to energy of 180 keV/u, is transported to DTL by a set of quadrupole magnets with field gradients less than 17 T/m. The purpose of MEBT section is to match the beam to DTL in all phase spaces along with suitable space for beam diagnostics. A double gap 48.5 MHz spiral buncher is used at the middle of MEBT section to provide phase matching with the DTL. The beam optics is shown in figure 23 along with 3D view of beam optical components. Hardware design of all the quadrupole magnets along with support stands, and vacuum chambers has been completed in collaboration with Danfysik.

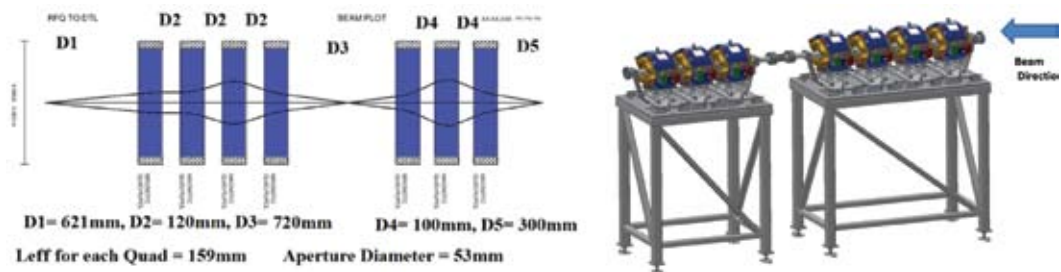


Fig. 23 Beam optics of MEBT section using TRACE 3D code along with its 3D view

## III. High energy beam transport section (HEBT)

HEBT consists of two types of achromat, type I and II. Type I has 7 quadrupoles and 2 dipoles ( $45^\circ$ ) whereas type II has 8 quadrupoles and 2 dipoles ( $45^\circ$ ). Hardware design has been performed in collaboration with Danfysik. Hardware design of the dipole magnet has been simulated using OPERA 3D code, to match the specifications as per beam optics. All the technical drawings have been completed for fabrication. The assembly of dipole and quadrupole magnets in different achromat configuration is a challenging task. A combined chamber has been designed for dipole and quadrupole magnets in the first achromat. A special chamber for the quadrupole singlet between the two dipoles of achromat type I has been designed to include vacuum pumps and diagnostic devices. Similarly, an integrated chamber for quadrupoles of achromat type II has been designed to provide a provision for inserting slits for charge state selection. Whole layout of the HCI along with its zoomed view of achromatic configuration are shown in figure 24.

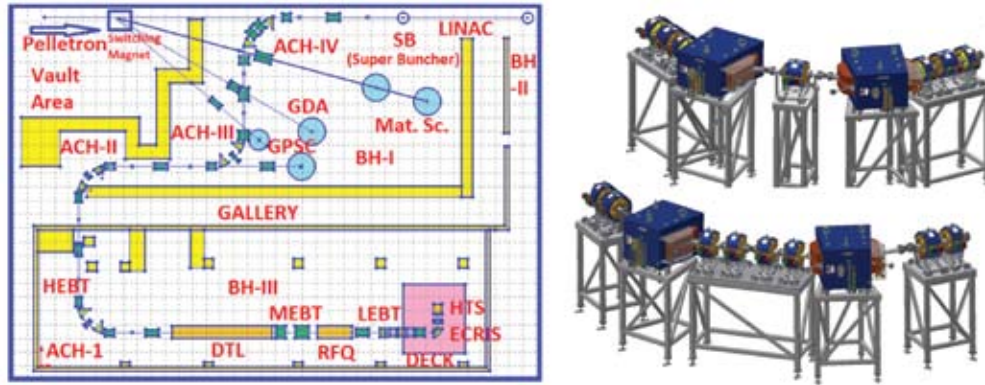


Fig. 24 Layout of the HCI and 3D view of achromats type I, II

#### 2.2.4.2 Fabrication of magnetic quadrupoles for LEBT section of HCI

Sarvesh Kumar, S.K.Saini and A.Mandal

Five magnetic quadrupoles having maximum field gradient of 3.85 T/m with aperture diameter of 78 mm, have been fabricated and preliminary testing has been performed. The effective length comes out to be 156 mm from magnetic field mapping data.



Fig. 25 Fabricated and tested magnetic quadrupoles

#### 2.2.4.3 Fabrication of fast Faraday cup for HCI

A coaxial type fast Faraday cup (FFC) is being designed to measure the time width of beam bunches. It is compact in size so as to fit in the spatial restrictions of the beam lines. A metallic solid stopper of a heavy element like tantalum is used to collect the beam. It is made of copper and 50  $\Omega$  impedance-matched to an SMA connector through a coaxial and conical geometry. A tungsten grid is positioned at few mm in front of the solid stopper. The diameter of the central conductor is tapered down to the diameter of SMA connector which is a coaxial RF connector having 50  $\Omega$  impedance. The inner and outer diameters are 25 mm and 57.5 mm respectively, whereas the inner and outer angles are 15° and 33.5° respectively to match input and output impedance to 50  $\Omega$ . The design parameters of FFC are shown in table 1 and its geometry along with S-parameters analysis are displayed in figure 26.

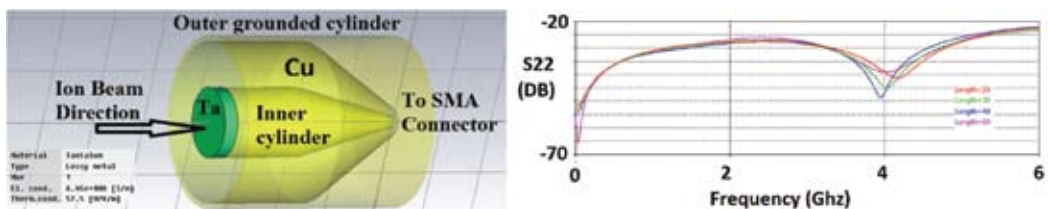


Fig. 26 Geometry of fast Faraday cup (calculated using the code CST MWS) and S parameters analysis for variable longitudinal lengths of coaxial circular conductor

**Table 1 : Design parameters of fast Faraday cup**

Beam Size	$\leq 1$ cm
Rise time of the Pulse	$\leq 1$ ns
Beam Current	$\leq 100$ $\mu$ A
Beam Energy	$\leq 180$ keV/u
Beam Power	$\leq 1$ kW
Bandwidth	1 Ghz
Input and Output impedances	50 $\Omega$

## 2.3 CRYOGENICS AND APPLIED SUPERCONDUCTIVITY LAB

A Choudhury, J Chacko, J Antony, M Kumar, S Babu, S Kar, S Sahu and T S Datta

The longest LINAC run was initiated with all five beam line cryomodules by using the new helium refrigerator (Linde make, LR280) along with the new section of the liquid helium distribution line by the end of November 2012. This run continued till March 2013. No further LINAC run was performed in this year. The superconducting quadrupole magnet for HYRA was completed and tested successfully in this year. Condenser along with the storage dewar for table top liquid nitrogen plant of capacity 64 liters/day was developed and initial test was performed successfully. This program is funded by BRNS.

### 2.3.1 Cryogenics for superconducting LINAC

A long run of the Linde (LR280) helium refrigerator machine spanning 105 days was performed with minimum interference from the operator. In addition, there were a few stand alone runs with the old CCI machine for performance test of QWR cavities and new low  $\beta$  cavity, developed earlier in this year. A couple of runs for the new plant were dedicated for minimizing the cool down time of the Linde machine and to measure refrigeration capacity at various discharge pressure. The cool down time was minimized from existing 25 hours to 17 hours with properly defined minimal intervention from the operator. Measured refrigeration capacity was more than 500 W without  $\text{LN}_2$  precooling. The measured value at different discharge pressure is shown in figure 27. We could not reach above 700 Watt with  $\text{LN}_2$  precooling as the respective heater, immersed in LHe, was burnt out. On extrapolation, it can be seen that the available refrigeration capacity at 13 bar discharge pressure will be more than 900 W@4.5K with  $\text{LN}_2$  precooling.

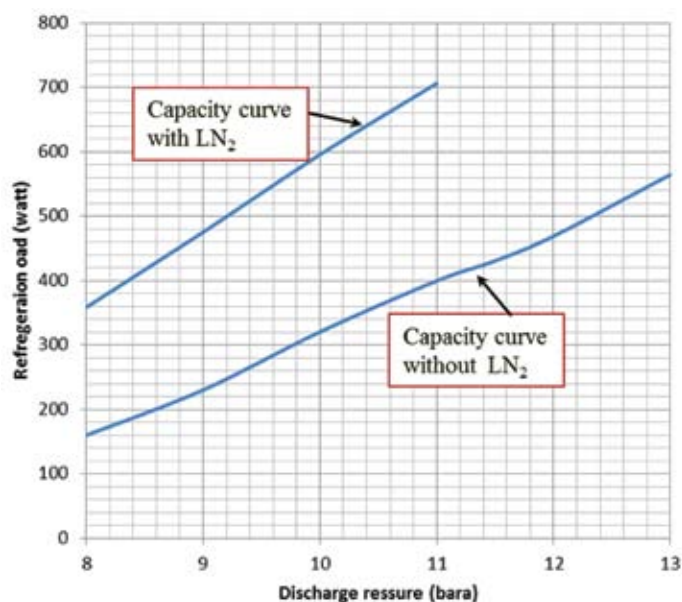


Fig. 27 : Design parameters of fast Faraday cup

The total LN<sub>2</sub> consumption in this period was 3,41,200 l, out of which 1,29,200 l was procured from external supply. The external procurement of LN<sub>2</sub> reduced due to rearrangement of the liquid nitrogen supply to the cryomodules (for the LINAC run) by using both the cryogenerators and utilizing the maximum capacity of the heat exchanger.

The cryogenics data acquisition system (CADS) has also undergone some improvement. PID control functions of the cryogenic control valves have undergone some changes for finer control of the valves which will help in reducing pressure fluctuation of the helium vessel of the cryostats. Use of CADS has allowed uninterrupted running of the cryogenic control system very efficiently with minimum human intervention.

### 2.3.2 Superconducting quadrupole magnet for HYRA

A superconducting quadrupole doublet magnet (SQDM) with a field gradient of 20 T/m and room temperature bore of 200 mm diameter was required for HYRA. To have an ever-cooled operation, it was planned to be fitted with a Sumitomo make 1.5 W@4.2K cryocooler. All the individual components like magnet, helium vessel, 60 K thermal copper shield and the vacuum jacket were put together at IUAC. The HTS current lead and the cryocooler were later integrated with helium vessel and vacuum jacket assembly. The completely assembled magnet is shown in figure 28. The magnet assembly, with a total weight of 2000 kg was cooled down in a controlled manner from 300 K - 4.2 K (without LN<sub>2</sub> precooling) by using the cryocooler in the initial phase and then with 2500 l LHe in batch filling. The shield temperature stabilized at 60 K. Both magnets were charged upto 70 A and available refrigeration capacity of 1.5 W was enough to maintain the LHe level. The cool down profile of the cryostat is shown in figure 29.

Magnetic field mapping was done by using Hall probes and the measured field profile is shown in figure 30. We also observed a quench when current exceeded 75 A. A detailed analysis of quench revealed that higher contact resistance at the mechanical junction (between HTS and LTS current leads) and insufficient conduction cooling are the sources of quench. Measures are being taken to improve conduction cooling in that region. The magnet was kept cooled for 4.5 months at 85% LHe level without any additional top up. This type of ever-cooled superconducting quadrupole magnet has been successfully designed and developed indigenously for the first time in India.



Fig. 28 Superconducting Quadrupole Doublet Magnet

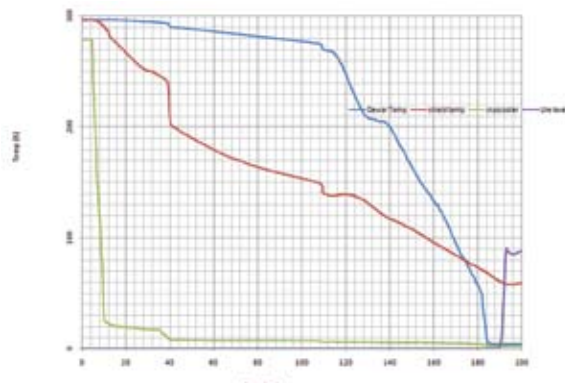


Fig. 29 Cool down curve of superconducting quadrupole doublet magnet

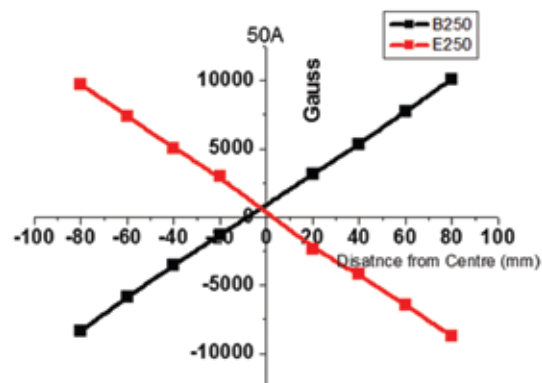


Fig. 30 Magnetic field profile of superconducting quadrupole doublet magnet

### 2.3.3 Development of a table top LN<sub>2</sub> plant

Our project proposal on development of a table top liquid nitrogen plant (capacity 60 l /day) by using a single stage cryocooler and condenser was approved by the BRNS. A special type of LN<sub>2</sub> dewar, with a wide neck of diameter 150 mm, was designed and fabricated with the help of M/s Vacuum Technique, Bangalore. The same is shown in figure 31. The GM cryocooler of capacity 260 W@80K (from M/s Cryomech, USA) along with the copper cryo-condenser was integrated with the dewar. In the first trial, the measured production rate was 64 l per day and the total cool down time was 9.5 hours. At present, the feed gas is pure nitrogen. The air separation module to generate pure nitrogen from air by using membrane is under progress.

### 2.3.4 VTI for indigenously developed cryo-free superconducting solenoid magnet

In continuation of earlier success on cryo-free 6 T superconducting solenoid magnet, DST approved another project on the development of a variable temperature insert (VTI) using a separate cryocooler. Both facilities together will enhance the measurement range from 4 K - 300 K in sample space with 0-6 T variable magnetic field. Design of the system has been completed and fabrication is in progress. A schematic design of the VTI setup is shown in figure 32. A detailed thermal analysis of quench and current lead characteristics on cryo-free magnet have been studied and published in a journal.



Fig. 31. LN<sub>2</sub> dewar with cryocooler

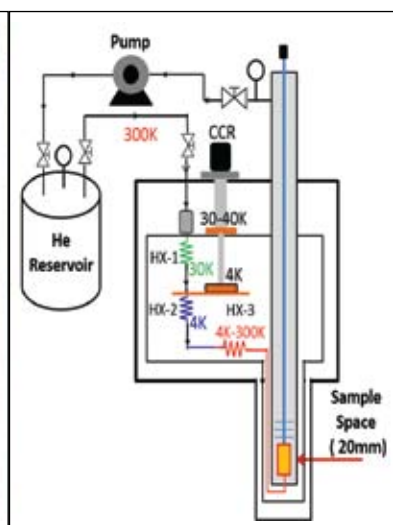


Fig. 32. Schematic diagram of the VTI cryostat

## 2.4 ELECTRONICS FOR CRYOGENICS: LAB ACTIVITIES

Joby Antony and D.S.Mathuria

**CADS:** The project CADS, stands for complete automation of distribution system, is to automate the complete cryogenic distribution system at IUAC using Ethernet based embedded instruments developed in-house. These cryogenic meters were designed out of COTS components with analog-sensor-front-end and webserver firmware for control & readout functions. All the instruments named as web sensors, each specific to a particular type of sensor-actuator combination, is now deployed across Cryogenic LAN. The production of SMD boards was completed using the CAM reflow soldering process. These devices have emergency switches by which each device can be taken to emergency mode and then operator can take control to local switches and pots. In case of communication failure, every device can be rebooted remotely.

### The works completed last year are

Hardware & Firmware design and implementation of following six types of instruments distributed across Buncher cryostat, Linac cryostat1, linac cryostat2, Linac Cryostat3, ReBuncher Cryostst, gas management systems, New refrigerator area. The electrical cabling and LAN cabling were completed. The complete control software is developed in Labview and put into operation in cryogenic control room.

Following are five different types of instruments,

#### a) LHe level servers for Superconducting level sensors & actuator controls over WEB

This instrument is an embedded device which is built with dedicated analog front-end electronics for Liquid helium level sensing, using super conducting level gauges, and the digital circuitries to work as globally accessible distributed web servers for remote monitoring & closed loop controls. The actuators attached to this device are proportional valves and solenoid valves for automatic and PID controls to work either in local or remote mode of operation. Each device has its own IP address for unique identification with a built-in 320x240 graphical display with resistive touch interface to view the information locally. A 4x3 keypad is used for configuring the parameters. The device data can be accessed and controlled from any PC running a web client. The calibrated physical variables are directly accessed using remote procedure calls (RPC)

which are implemented in firmware. The user with a remote PC can read and write any variable data using a simple web browser running on any OS (windows/linux) without any prior programming knowledge. API support is extended for Labview, c, c++ etc. Each device also has an IP controlled PID controller card built in-house which are attached as daughter boards with added remote reboot feature. Thus, overall, it makes the “Sensor over web” a reality. Each board is a 4 layer design with smd components. The boards are manufactured using the pick and place re-flow process. The advantage of this kind of system is that IP addressable devices can be distributed at many different geographical locations across globe and can be accessed by single/multiple clients. Since the device is built-around ethernet, wi-fi mobiles can also be used instead of PCs in a local wi-fi network just by adding a wi-fi router. A USB and CAN interface is also provided for future use.



**b) LN2 level servers for Capacitive level sensors**

This instrument is built with dedicated analog front-end electronics for Liquid nitrogen level sensors, using capacitive level gauges, and the digital circuitries to work as distributed webservers for remote monitoring & closed loop controls. They can work either in local or remote mode of operation. This device has built-in circuitry called “cable capacitance compensator” which is a unique feature and hence they can be mounted far off from sensors by using a long lemo cable. The actuators attached to this device are proportional valves and solenoid valves for automatic and manual controls. All other features and implementations like PID etc are similar to the LHe meter explained above.

**c) Web-switch for AC power controls**

These are multi channel e-plugs with 5/15A/230V AC sockets designed to work like “remote AC plugs” operated through WEB. Thus heaters/pumps can be connected to each socket and can be controlled over WEB. ON/OFF status of each powered device is displayed on display screen. Such many web-switches can be distributed across a network using Ethernet. The advantage of this kind of device is that each socket is identified by a name which is displayed on a display screen e.g Rotary pump1 ON, heater1 OFF etc. All other features and implementations like PID etc are similar to the LHe meter explained above.

**d) Device servers for cryogenic temperature & pressure measurements**

This instrument is built with dedicated analog front-end electronics for cryogenic temperature sensors [4.2 to 300k] or pressure sensors [-14.7 to +14.7 PSI], and the digital circuitries to work as globally accessible web servers for remote monitoring. The precise current sources and programmable instrumentation amplifiers are built inside the front-end analog processing electronics. All other features and implementations like PID etc are similar to the LHe meter explained above.

**e) Cryogenic Tank & vacuum server**

This instrument is built with dedicated analog front-end electronics for cryogenic tank temperatures and pressures [-14.7 to +14.7 PSI], vacuum measurements etc. and the digital circuitries to work as globally accessible web servers for remote monitoring of Cryogenic tank.

**The user friendly GUI software for control room**



Fig: CADS instruments during tests at lab

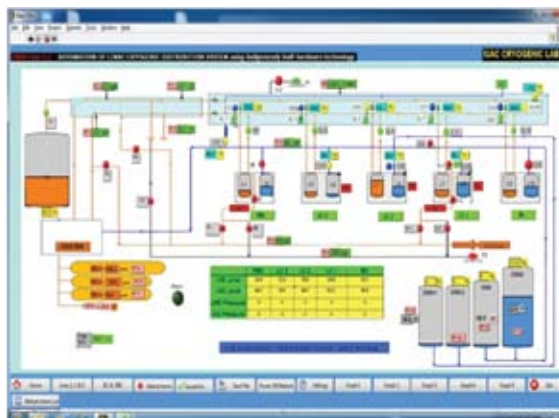


Fig: The control user interface

The control and data acquisition software has 50 trends, each of which has history duration of 24 hours. The trend data files are created automatically at 12:00 AM. A separate data logger is also provided to log all analog & digital data for infinite duration. Every data is compatible to EXCEL. Alarm features are user programmable for low and high limits. A health monitoring utility has been added to test the health of each device periodically and report to users. PID dialog boxes and other operational features is very user friendly.



Fig: A 24 hour trend view of proportional valves controlled by PID